Development of newborn and 1-year-old reference phantoms based on polygon mesh surfaces

V F Cassola[1], R Kramer[1], V J de Melo Lima[2], C A B de Oliveira Lira[1], H J Khoury[1] , J W Vieira[1,3,4] and K Robson Brown[5]

[1]Department of Nuclear Energy, Federal University of Pernambuco, Avenida Professor Luiz Freire 1000, CEP 50740-540, Recife, Pernambuco, Brazil

[2]Department of Anatomy, Federal University of Pernambuco, Recife, Pernambuco, Brazil

[3] Federal Institute of Education, Science and Technology of Pernambuco, Recife, Brazil

[4]Polytechnic School of Pernambuco, University of Pernambuco, Recife, Brazil

[5]Imaging Laboratory, Department of Archaeology and Anthropology, University of Bristol, Bristol, UK

E-mail: rkramer@uol.com.br

Statement of provenance:
'This is an author-created, un-copyedited version of an article accepted for publication in the Journal of Radiological Protection. IOP Publishing Ltd is not responsible for any errors or omissions in this version of the manuscript or any version derived from it. The definitive publisher authenticated version is available at doi:10.1088/0952-4746/33/3/669.'

Abstract

The purpose of this study is the development of paediatric reference phantoms for newborn and 1-year-old infants to be used for the calculation of organ and tissue equivalent doses in radiation protection. The study proposes a method for developing anatomically highly sophisticated paediatric phantoms without using medical images. The newborn and 1-year-old hermaphrodite phantoms presented here were developed using 3D modelling software applied to anatomical information taken from atlases, textbooks and images provided by the Department of Anatomy of the Federal University of Pernambuco. The method uses polygon mesh surfaces to model body contours, the shape of organs as well as their positions and orientations in the human body. Organ and tissue masses agree with corresponding data given by the International Commission on Radiological Protection for newborn and 1-year-old reference children. Bones were segmented into cortical bone, spongiosa, medullary marrow and cartilage to allow for the use of μCT images of trabecular bone for skeletal dosimetry.
Anatomical results show 3D images of the phantoms' surfaces, organs and skeletons, as well as tables with organ and tissue masses or skeletal tissue volumes. Dosimetric results present comparisons of organ and tissue absorbed doses or specific absorbed fractions between the newborn and 1-year-old phantoms and corresponding data for other paediatric stylized or voxel phantoms. Most differences were found to be below 10%.

1. Introduction

In the community of radiation protection, exposure of children to medical external ionizing radiation became a concern first, because for given irradiation conditions children often receive higher organ

and tissue absorbed doses than adults and second, because children have greater life time risks per unit absorbed dose of radiation. Consequently, the life time cancer mortality attributable to exposure to ionizing radiation is significantly higher in children than in adults (Brenner et al 2001). Quantification of radiation risks requires knowledge about the absorbed dose to radiosensitive organs and tissues which cannot be measured in vivo. However, computational exposure models consisting of Monte Carlo (MC) computer codes connected to virtual human phantoms can be used to resolve this problem by simulating the exposure of the human body and calculating organ and tissue absorbed doses normalized to measurable quantities. Therefore, paediatric virtual anatomical models represent an important part of any human phantom development program.

Initially, paediatric mathematical or stylized phantoms representing newborns, 1-, 5-, 10- and two 15-year-old children were developed by Cristy (1980) and Cristy and Eckerman (1987) from the Oak Ridge National Laboratory (ORNL). The ORNL series of paediatric phantoms were later revised by Han et al (2006) through the introduction of additional organs and by updating tissue compositions. The revised ORNL phantoms have been used by Lee et al (2007a) to study the impact of the latest Recommendations of the International Commission on Radiological Protection (ICRP) (ICRP 2007) on the effective dose.

The development of tomographic or voxel phantoms actually began with the design of paediatric models. BABY and CHILD based on CT images of an 8-week-old and of a 7-year-old child, respectively, which were developed by Williams et al (1986) and Zankl et al (1988) to calculate organ and tissue absorbed doses for X-ray procedures. Later, comprehensive studies of paediatric voxel phantoms for various ages were carried out at the University of Florida (UF). Initially, head and torso phantoms were developed which later received arms and legs (Lee et al 2005, 2006), as well as organ and tissue masses adjusted to reference data given by ICRP89 (2002).

Hybrid computational models represent an important step in paediatric phantom development. Based on medical images acquired by CT or NMR from real bodies, this method then applies 3D modelling software to these images to create organs and body contours of unprecedented anatomical realism, better achievable than in voxel phantoms, but which can easily be changed, like in stylized phantoms. Lee et al (2007b) from the UF were the first to present a hybrid phantom for the newborn and since then a whole family of UF paediatric hybrid phantoms has followed (Lee et al 2008, 2010). Based on whole body NMR images taken from volunteers, Christ et al (2010) also developed hybrid paediatric phantoms for a 5-year-old boy and an 11-year-old girl. A comprehensive overview on phantom development is given by Xu and Eckerman (2010) which also includes paediatric phantoms, such as those developed by Nagaoka et al (2008) by transforming adult bodies into paediatric anatomies for 7, 5 and 3 years of age.

The Department of Nuclear Energy at the Federal University of Pernambuco (DEN/UFPE) has been developing human phantoms over the last ten years (Kramer et al 2003, 2004, 2006a). The latest edition of the male and female adult, ICRP89-based, posture-specific phantoms, called MASH and FASH (Cassola et al 2010a, 2010b, 2011), as well as 5- and 10-year-old paediatric phantoms (de Melo Lima et al 2011) have been developed from anatomical atlases, textbooks and images from the Department of Anatomy of the UFPE applying 3D modelling software based on polygon mesh surfaces, i.e. without using medical tomographic images of patients or volunteers. In all phantoms, skeletal dosimetry employs a method based on μCT images of trabecular bone which was developed at the DEN in collaboration with the Imaging Laboratory, Department of Archaeology and Anthropology at the University of Bristol (Kramer et al 2006b, 2007, 2009, 2010, 2011, 2012).

The purpose of this study is to extend the mesh phantom library of the DEN to paediatric hermaphrodite phantoms for newborn and 1-year-old infants. Voxelized versions of these phantoms will be used for dosimetric calculations and the results will be compared with similar data for other paediatric phantoms.

2. Materials and methods

Modelling the human anatomy for the purposes of radiation protection without using medical images from patients or volunteers requires first, a comprehensive anatomical description of human anatomy, especially of all the radiosensitive organs and tissues considered at risk by the International Commission on Radiological Protection (ICRP); and second, 3D objects representing the human body surface, organs and tissues; and third, software suitable to create and/or edit these 3D objects. With respect to the description of the human paediatric anatomy the following sources have been consulted: ICRP Publication 89 (2002) and 70 (1995) for reference total body mass, height as well as organ and tissue masses, densities and tissue compositions for newborn and 1-year-old infants; additionally ICRU46 (ICRU 1992) for tissue densities; the report AnthroKids (Snyder et al 1977) for anthropometric parameters, anatomical atlases and textbooks (Gray 1977, Netter 1999, MacGregor 2000, Moore and Dalley 2007) as well as images of a newborn cadaver provided by the Department of Anatomy of the UFPE for the definition of shapes, positions and orientations of organs within the body and relative to each other. The body surfaces were modelled from scratch, while organs of the 5-year-old DEN phantoms (de Melo Lima et al 2011) were modified to the appropriate size for the two infants.

The main computational tool used in this study was Blender 2.49b, a free, open source software for modelling, animating and other applications, such as the support for a variety of geometric primitives, including poly meshes, Bezier curves, non-uniform rational B-spline surfaces (NURBS) and digital sculpting which allows for the creation, editing and voxelization of 3D objects (Rosendaal 2009). Figure 1 shows the user interface of Blender 2.49b with a set of internal organs for the newborn. In this image the user is modelling the stomach, shown in brown colour with yellow vertices. Length and direction of the vertices can be changed by moving the yellow dots, called control points. On the bottom right, Blender shows the actual volume. Apart from Blender, the software Image J (http://rsbweb.nih.gov/ij/) was used for the segmentation of skeletal tissue volumes and of the contents in walled organs.

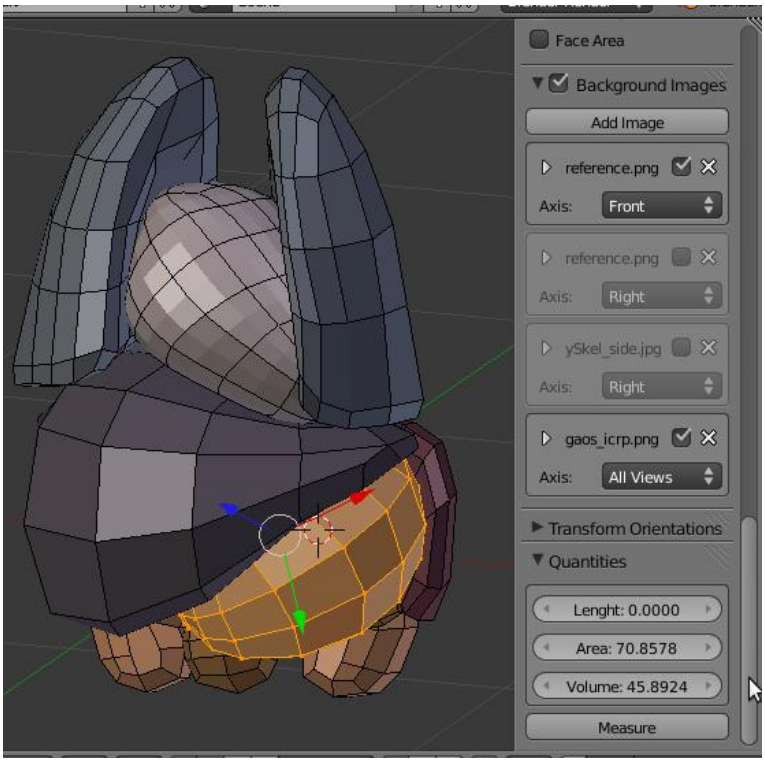

Fig 1. Blender user interface showing polygon mesh surfaces for internal organs for the newborn with the stomach highlighted in brown. Vertices in yellow can be changed at control points to model shape the and volume of the organ. The resulting volume is indicated on the bottom right.

2.1 Body surface

First, a basic polygon mesh human body surface model, shown in figure 2, was created with Blender, including anatomical structures, such as ears, mouth, nose, etc. and then adjusted to newborn and 1-year-old anthropometric dimensions using ICRP89 (ICRP 2002) and AnthroKids (Snyder et al 1977).

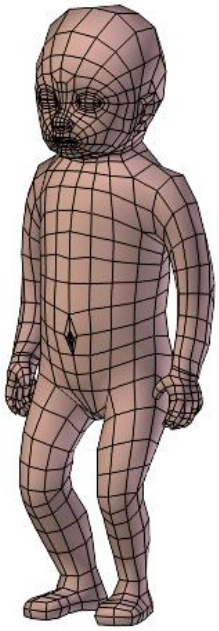

Fig 2. Basic polygon mesh surface model created with Blender 2.49b (Rosendaal 2009).

2.2 Skeleton

The skeletons were modelled based on a method developed earlier (de Melo Lima et al 2011). First, the skeleton of a 5-year-old phantom was scaled down to fit into the newborn and the 1-year-old body surfaces developed under 2.1. Then the sizes and the positions of the bones were changed according to anthropometric paediatric data for different body parts taken from Snyder et al (1977). After voxelization, using Image J the skeletons were segmented into cortical bone, medullary marrow, cartilage and spongiosa (which is trabecular bone filled with marrow), to allow for the use of μCT images of trabecular bone for skeletal dosimetry. Cartilage also includes the unossified regions between bones found in skeletons of infants. Figure 3 shows these regions for the skull, as an example. The process of ossification is completed by the age of 4. The skeletal tissue volumes were calculated using a method similar to that described earlier for the adult phantoms (Kramer et al 2010, 2012). This method uses quantities taken from or calculated based on data found in ICRP publications to determine bone-specific tissue volumes. Age-specific skeletal tissue masses were taken from table 2.8 of ICRP89 (ICRP 2002) and are shown in table 1 together with their densities and the calculated target volumes. Red (active) bone marrow (RBM) mass fractions taken from table 9.4 in ICRP89 (ICRP 2002), cellularity factors taken from table 41 and bone mass fractions calculated from tables 8 and 9 in ICRP70 (ICRP 1995) are shown in table 2 together with mass ratios between cortical and trabecular bone for adults, taken from table 9.3 in ICRP89 (ICRP 2002), because paediatric data are currently not available for these quantities in ICRP documents. The data presented in tables 1 and 2 were used to calculate bone-specific volumes for cortical bone, spongiosa, and cartilage in the paediatric skeletons which serve as target volumes for skeletal segmentation.

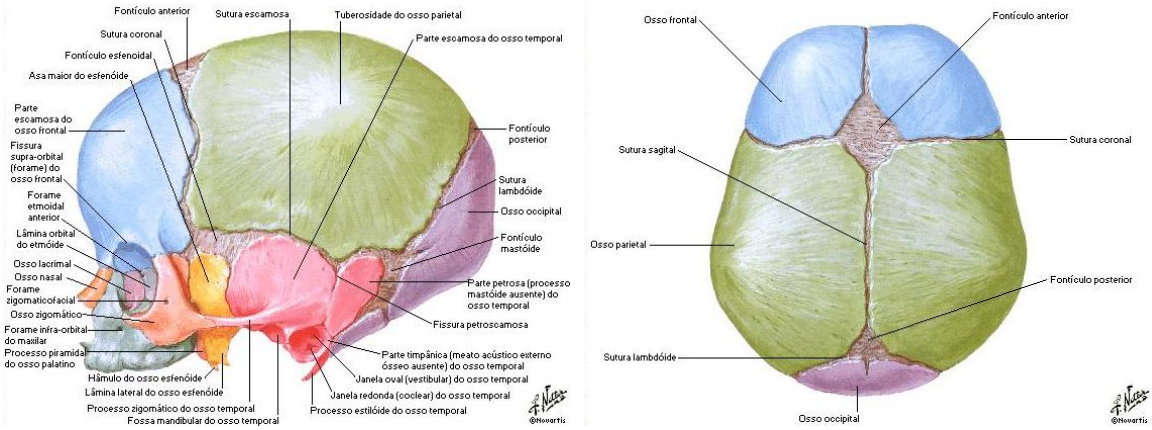

Fig 3. The skull of a newborn lateral view and view from the top. The flat bones of the skull are separated by areas of fibrous connective tissue (unossified regions), allowing for cranial expansion and the distortion of the skull during birth (Netter 1999).

The calculation of the volume of the medullary cavities in the newborn skeleton was achieved by applying the following procedure: First, the RBM volumes in the long bones were calculated with ICRP data from table 1 and 2. Second, using information from table 5 of the work of Pafundi et al (2009), the distribution of the bone-specific RBM volume between shafts, proximal and distal spongiosa was determined. Finally, using data from table 12 of Pafundi et al (2009) cavity length and diameter were calculated assuming cylindrical cavities. Figure 4 shows the voxelized skeleton of the newborn hermaphrodite phantom with an amplification of the left femur and a longitudinal cut through the bone highlighting the segmented medullary cavity in red.

Tab 1. Tissue masses, densities and calculated target volumes for the newborn and 1-year-old skeletons. Data taken from ICRP89 (ICRP 2002) and ICRU46 (ICRU 1998)

	Newborn			One year		
Skeletal region	ICRP89 mass (g)	ICRU46 density (g cm^{-3})	Target volume (cm^3)	ICRP89 mass (g)	ICRU46 density (g cm^{-3})	Target volume (cm^3)
Bone, cortical	135	1.65	81.8	470	1.66	283.1
Bone, trabecular	35	1.65	21.2	120	1.66	72.3
Bone, total	170	1.65	103.0	590	1.66	355.4
Marrow, active (red)	50	1.03	48.5	150	1.03	145.6
Marrow, inactive (yellow)	0	0.98	0.0	20	0.98	20.4
Cartilage	130	1.10	118.2	360	1.10	327.3
Teeth	0.7	2.75	0.3	5	2.75	1.82
Miscellaneous	19.3	1.03	18.7	45	1.03	43.7
Total skeleton	370	1.28[a]	288.7	1170	1.31[a]	894.4

[a] calculated

Tab 2. Bone mass fractions, RBM mass fractions and cellularity factors for the newborn and 1-year-old skeletons. Mass ratios between cortical and trabecular bone are for the adult skeleton. The quantities were taken from or calculated based on data found in ICRP89 (ICRP 2002) and ICRP70 (ICRP 1995)

Skeletal region	Newborn Bone mass fraction	Newborn RBM mass fraction	Newborn Cellularity factor	1 year Bone mass fraction	1 year RBM mass fraction	1 year Cellularity factor	Adult Mass ratio of bone cortical / trabecular
Wrist and hand bones	0.019	0.036	1.00	0.017	0.019	0.50	95 / 5
Radii and Ulnae	0.037	0.025	1.00	0.034	0.025	0.89	85.5 / 14.5
Humeri, upper half	0.024	0.023	1.00	0.022	0.024	0.95	80 / 20
Humeri, lower half	0.024	0.023	1.00	0.022	0.023	0.89	80 / 20
Ribs	0.077	0.092	1.00	0.078	0.089	0.95	94 / 6
Sternum	0.006	0.000	1.00	0.006	0.008	0.95	94 / 6
Scapulae	0.022	0.027	1.00	0.020	0.027	0.95	94 / 6
Clavicles	0.007	0.008	1.00	0.007	0.008	0.95	94 / 6
Cervical vertebrae	0.020	0.034	1.00	0.021	0.028	0.95	25 / 75
Thoracic vertebrae	0.052	0.083	1.00	0.052	0.084	0.95	25 / 75
Lumbar vertebrae	0.043	0.024	1.00	0.044	0.043	0.95	34 / 66
Sacrum	0.025	0.001	1.00	0.026	0.024	0.95	75 / 25
Cranium	0.410	0.270	1.00	0.418	0.251	0.95	95 / 5
Mandible	0.041	0.025	1.00	0.042	0.024	0.95	95 / 5
Pelvis	0.036	0.092	1.00	0.036	0.111	0.95	90 / 10
Femora, upper half	0.039	0.037	1.00	0.038	0.041	0.95	67 / 33
Femora, lower half	0.039	0.037	1.00	0.038	0.039	0.89	67 / 33
Tibiae, fibulae, patellae	0.056	0.080	1.00	0.056	0.087	0.89	75 / 25
Ankle and foot bones	0.023	0.083	1.00	0.023	0.047	0.50	95 / 5

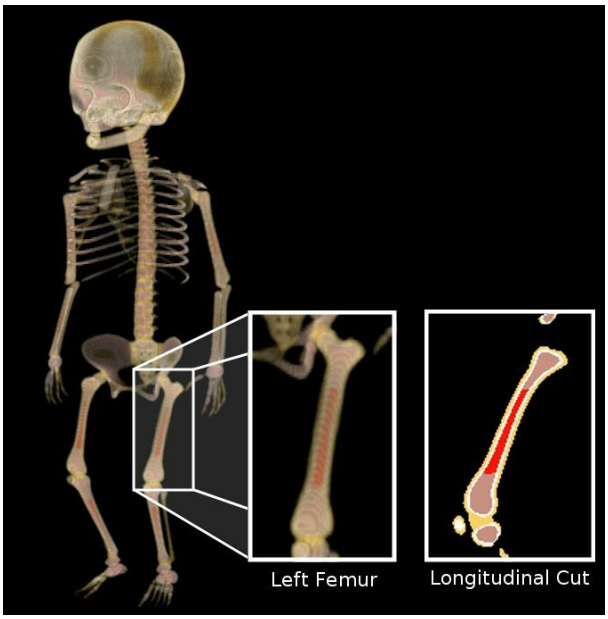

Fig 4. Voxelized newborn skeleton with amplified view of the left femur, plus a longitudinal cut through the bone highlighting the segmented medullary cavity in red.

Cavity lengths for the 1-year-old long bones were calculated by scaling the newborn cavity lengths with the ratio between corresponding bone lengths of the two skeletons. Using the diameter ratio of the bones and a similar method, the cavity diameters for the 1-year-old long bones were determined. As the 1-year-old skeleton already contains yellow (inactive) bone marrow (YBM), the cellularity factors from table 2 were additionally used to determine the volumes of RBM and YBM in the medullary cavities. μCT images of trabecular bone for newborn and 1-year-old skeletons are currently not available. Therefore, μCT images of the 5-year-old phantoms, which were derived from images for adults (de Melo Lima 2011), were used in the spongiosa of the newborn and 1-year-old skeletons.

2.3 Organs and soft tissues

Using the reference masses from table 2.8 of ICRP89 (ICRP 2002) and the reference densities from ICRP89 and ICRU46 (ICRU 1998), the target volumes for each organ and tissue for newborn and 1-year-old infants were calculated. The organs of the 5-year-old phantoms (de Melo Lima et al 2011) were then imported with Blender into the body surface and changed to match the target volumes using anatomical atlases and textbooks, as well as cadaver images and an image from page 70 of ICRP89, which can be seen in figure 5. This process was first employed for the newborn hermaphrodite phantom (P00), and subsequently the P00 results were used for modelling the organs of the 1-year-old hermaphrodite phantom (P01).

Breast tissue is not mentioned among reference masses in table 2.8 of ICRP89 for humans under 15 years, but an average value of 0.09 g for the breasts of newborns is given on page 211. The breast mass for the 1-year-old phantom was calculated by scaling up the ratio between the body masses for 1-year-old and newborn: 0.09 g x (10kg/3.5kg) = 0.26 g for the 1-year-old breast mass.

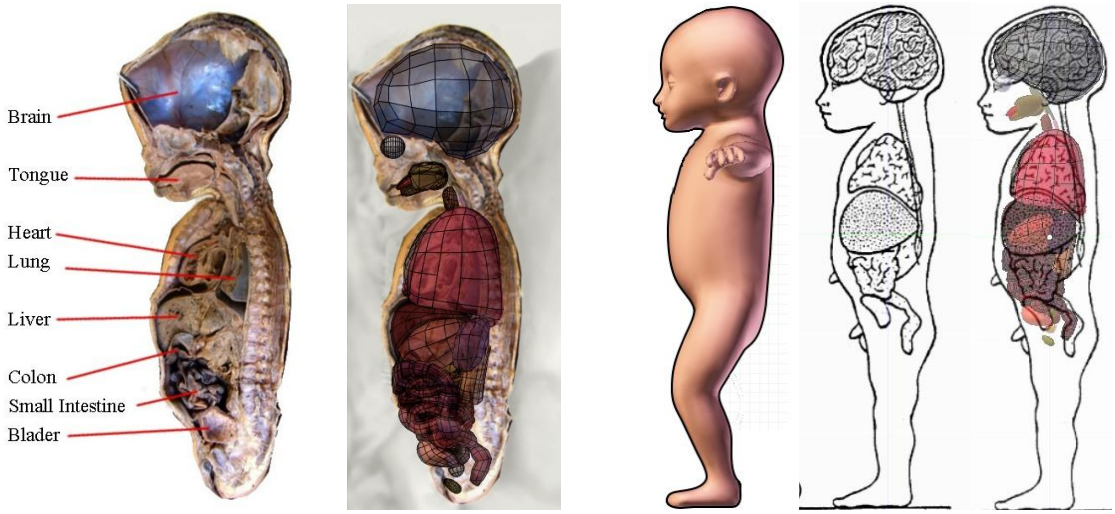

Fig 5. From left to right: Image of a new born formalinized cadaver from the department of anatomy of the UFPE, cadaver image imported into Blender and filled with mesh organs, UFPE newborn mesh body surface, ICRP89 newborn (ICRP 2002, page 70) and ICRP newborn imported into Blender and filled with mesh organs.

The brain was modelled to fit within the central cranial cavity. Other organs, such as the salivary glands, eyes, tongue, nasal cavity, larynx and pharynx were modelled using subdivision and digital sculpturing of Blender. The trachea and the oesophagus were designed using polygonal modelling. The lungs were adjusted to fill the thoracic cavity, but at the same time the positioning of the heart was taken into account. Tubular structures, such as small intestine and colon, were made using the editing tool “extrusion” of Bezier curves, a tool within the Blender software which allows modelling

winding tubes with defined widths and wall thicknesses. In addition, the masses and the physiological lengths were matched to the ICRP89 reference data.

Lymphatic nodes located on both sides of the central sagittal plane were designed as ellipsoids using the DupliVert tool provided by the Blender software. DupliVert comes from *Dupli*cation at *Vert*ices and represents a method which duplicates all vertices of the polygon mesh of an object. Non-symmetrical lymphatic nodes were designed as spheres. The lymphatic nodes have been modelled in the mesh phantoms at the armpit, at the groins, behind the knees, in front of the elbows, at the neck, at the face, around large the blood vessels of the throat and trunk, as well as around abdominal soft-tissue organs. According to footnote c of table 2.8 in ICRP89 "separable connective tissue and certain lymphatic tissues account for most of the remaining 4% of body mass". Using this statement and table 11.2 on page 217 of ICRP89 on connective tissue masses, the masses of the lymphatic nodes were calculated as 20 g and 50 g for the newborn and 1-year-old, respectively.

2.4 Voxelization

The hermaphrodite newborn (P00) and 1-year-old (P01) phantoms had to be voxelized for two reasons: First, the EGSnrc Monte Carlo code (Kawrakow and Rogers 2003), frequently used at the DEN/UFPE for dosimetric studies, cannot be connected with polygon mesh geometries and second, the μCT images to be used for skeletal dosimetry are voxelized matrices. The voxelization was achieved with the Blender software using cubic voxels of 700 μm, which, according to ICRP89 (ICRP 2002), is the total thickness of the skin for children up to 10 years of age. After voxelization, all surface voxels have the ID number for subcutaneous adipose tissue. The skin voxels were defined by re-tagging adipose surface voxels based on the following procedure: First, adipose voxels for which one of the 8 lateral neighbours is an air voxel are re-tagged as skin voxels. If the target volume for the skin was not achieved, which was usually the case for all mesh phantoms developed at the DEN earlier, then the procedure is repeated with the 26 lateral and diagonal neighbours until the target volume is met. This procedure may produce small areas with skin thicknesses made of 2 or 3 voxels in some regions with curved surfaces, such as the chin, the cranium, the hands and the feet. Using special plug-ins developed for Image J, the skeletons were segmented into cortical bone, spongiosa, cartilage and medullary cavities while stomach, intestines, urinary bladder and gall bladder were segmented into wall and contents only in the voxelized version of the phantoms.

2.5 Dosimetry

After voxelization, the paediatric phantoms P00 and P01 were connected to the EGSnrc MC code (Kawrakow and Rogers 2003) which is one of the best bench-marked MC codes for coupled photon/electron transport with a dynamic range of charged particle kinetic energies between a few tens of keV and a few hundred GeV, and of photon energies between 1 keV and several hundred GeV. Cut-off energies were 2 keV for photons and 20 keV for electrons outside the skeleton. Inside the skeleton, the electron cut-off energy was 5 keV. Organ and tissue absorbed doses were calculated as follows; first, for thorax examinations and will be compared with corresponding results for stylized phantoms (Seidenbusch et al 2008); second, for one liver CT scan and will be compared with corresponding data for the newborn voxel phantom BABY (Zankl et al 1993); and third, specific absorbed fractions (SAFs) were calculated and will be compared with the newborn NURBS-based phantom of the University of Florida (Pafundi et al 2010). All X-ray spectra used in this study have been taken from the catalogue published by Cranley et al (1997).

3. Results

3.1 Anatomy

3.1.1 The mesh phantoms

Views of the surface, of the bones with unossified regions for the skeleton and for the skull, and of the organs are shown for the newborn (P00) hermaphrodite mesh phantoms in figures 6 from left to right. Additionally in figure 6, the last image on the right shows the distribution of the lymphatic nodes in the newborn. Similar images are shown in figure 7 for the 1-year-old (P01) mesh phantom.

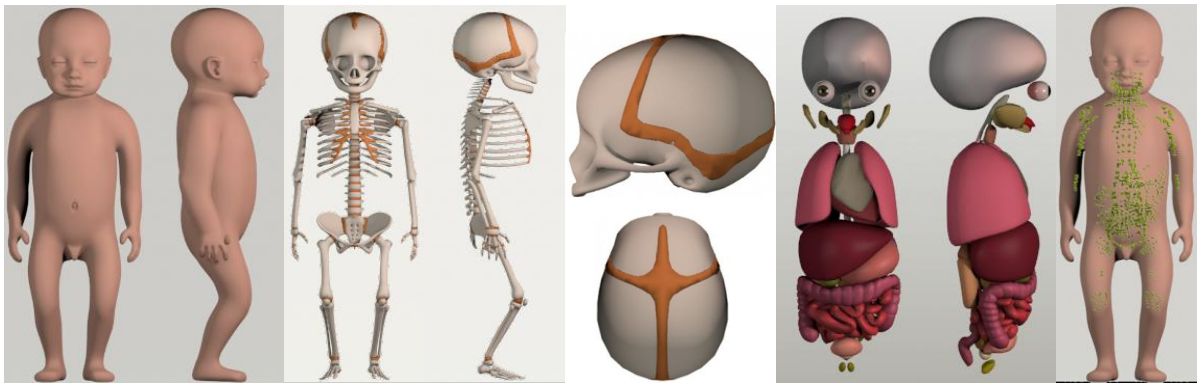

Fig 6. Newborn hermaphrodite mesh phantom P(00): Surface, skeleton, skull, organs and lymphatic nodes.

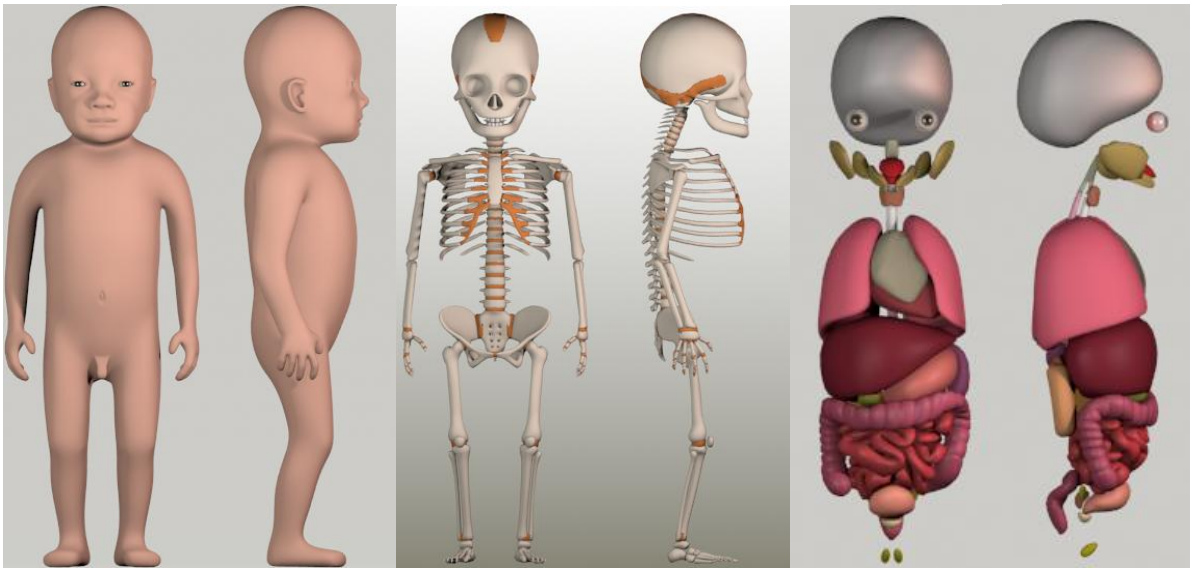

Fig 7. 1-year-old hermaphrodite mesh phantom (P01): Surface, skeleton and organs.

3.1.2 The voxel phantoms

The paediatric mesh phantoms P00 and P01 were voxelized with a cubic resolution of 700 µm. Figure 8 shows from left to right the voxel surfaces and skeletons of the newborn (P00) and the 1-year-old (P01) hermaphrodite phantoms, lymphatic nodes for the P00, and organs for the P01models. Due to

the high voxel resolution all anatomical details are well preserved. Segmentation of skeletal tissue volumes, walls of intestines, stomach, urinary bladder, gall bladder and final adjustments of organ and tissue masses were achieved in the voxelized versions of the phantoms. Table 3 shows some of the important properties. For comparison, ICRP89 reference standing heights are 51 cm and 76 cm and total body masses are 3.5 kg and 10 kg for the newborn and 1-year-old infants, respectively. Using the data shown in tables 1 and 2, the bone-specific skeletal tissue volumes for cortical bone, spongiosa, medullary marrow and cartilage have been calculated and segmented in the voxelized skeletons. They are shown in table 4 and 5 for the newborn and the 1-year-old skeletons, respectively.

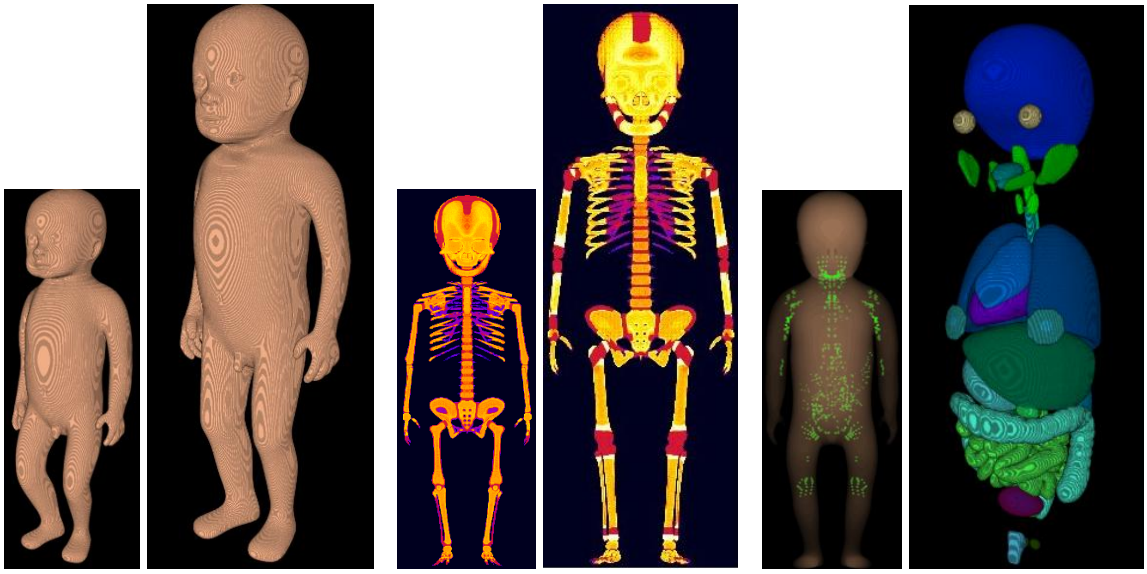

Fig 8. Voxelized phantoms from left to right: Surfaces and segmented skeletons showing cortical bone, cartilage and medullary cavities for P00 and P01, lymphatic nodes for P00 and organs for P01.

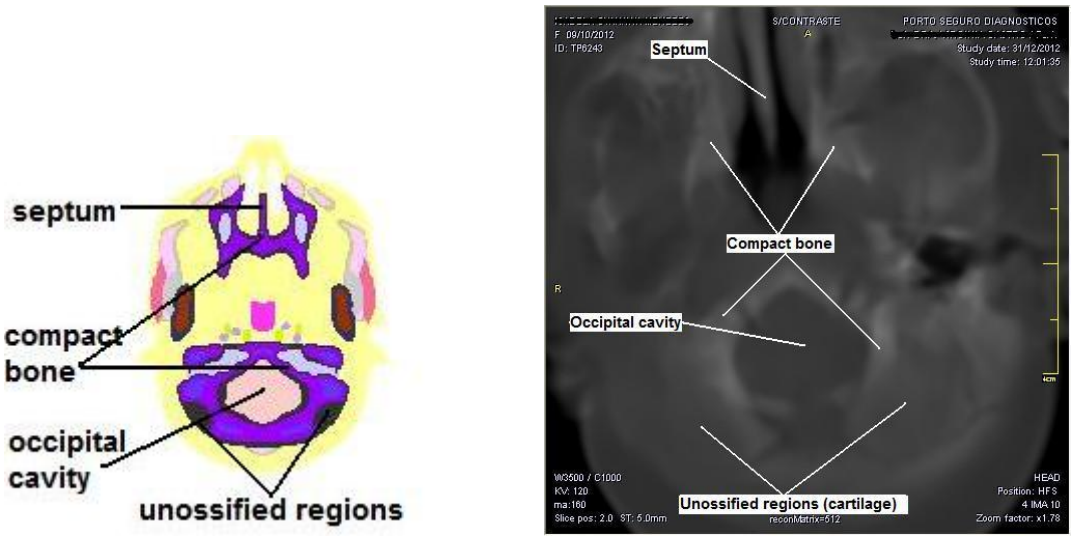

Fig 9. Transverse image of the newborn skull (P00 phantom) on the left. CT image of the same region of a 2 month old infant on the right (Courtesy by Porto Seguro Diagnosticos).

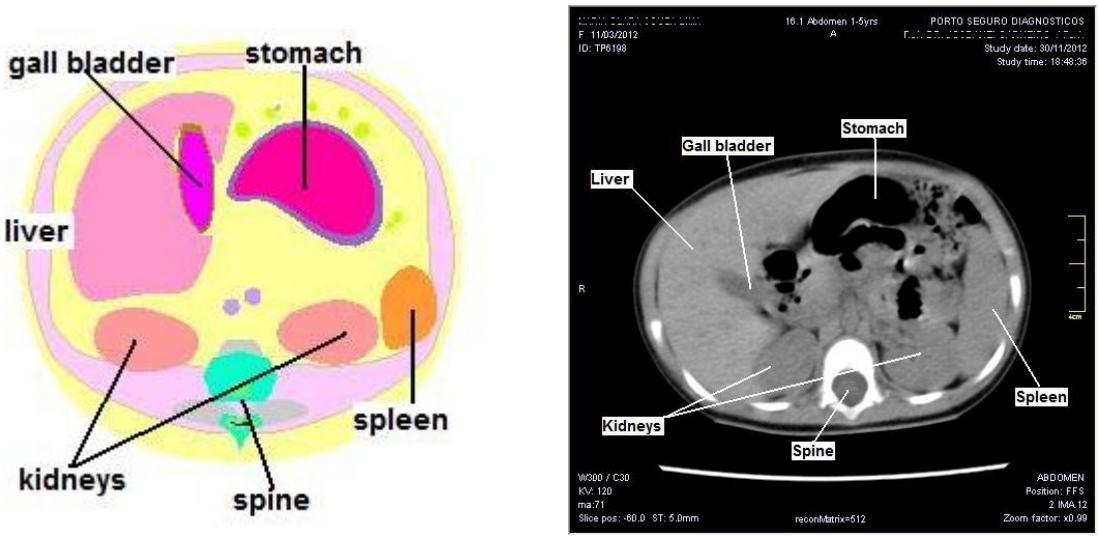

Fig 10. Transverse image of the 1-year-old abdomen (P01 phantom) on the left. CT image of the same region of an 8 month old infant on the right (Courtesy by Porto Seguro Diagnosticos).

At the Porto Seguro Diagnostic Medical Centre in Porto Seguro, Bahia, Brazil, 36 CT images were taken from the skull of a 2-month-old female because she had a facial trauma with nasal bleeding, while 38 CT images were taken from the abdomen of a 8-month-old female because she had to be submitted to a correction of the ureterocele. Figures 9 and 10 show comparisons between transverse images of the phantoms (P00 and P01) and corresponding CT images for 2-month and 8-month-old infants for the skull and the abdomen, respectively, which show reasonable anatomical agreement.

Tab 3. Properties of the hermaphrodite paediatric voxel phantoms.

	Newborn (P00)	1-year-old (P01)
Organs and tissues segmented	45	45
Voxel size (cm x cm x cm)	0.07 x 0.07 x 0.07	0.07 x 0.07 x 0.07
Number of columns	270	380
Number of lines	198	270
Number of slices	722	1083
Height (cm)	50.5	75.8
Total body mass (kg)	3.5	10

Tab 4. Bone-specific skeletal tissue volumes for the newborn skeleton calculated from the data shown in tables 1 and 2 and segmented in the newborn skeleton.

Newborn Skeletal region	Cortical bone (cm^3)	Spongiosa (cm^3)	RBM med (cm^3)	Cart/misc (cm^3)	Total (cm^3)
Wrist and hand bones	1.86	1.84		2.60	6.31
Radii and Ulnae	3.26	1.59	0.18	5.06	10.09
Humeri, upper half	1.98	1.39	0.22	3.28	6.87
Humeri, lower half	1.98	1.39	0.22	3.28	6.87
Ribs	7.45	4.94		10.54	22.94
Sternum	0.58	0.04		0.82	1.44
Scapulae	2.13	1.44		3.01	6.59
Clavicles	0.68	0.43		0.96	2.07
Cervical vertebrae	0.52	3.20		2.74	6.45
Thoracic vertebrae	1.34	8.05		7.12	16.50
Lumbar vertebrae	1.51	4.09		5.88	11.48
Sacrum	1.93	0.69		3.42	6.05
Cranium	40.13	15.22		56.11	111.46
Mandible	4.01	1.43		5.61	11.05
Pelvis	3.34	4.84		4.93	13.10
Femora, upper half	2.69	2.58	0.54	5.34	11.15
Femora, lower half	2.69	2.58	0.54	5.34	11.15
Tibiae, fibulae, patellae	4.33	4.75	0.58	7.66	17.32
Ankle and foot bones	2.25	4.15		3.15	9.55
	84.66	64.63	2.28	136.85	288.42
ICRP89 (no teeth)					288.70

Tab 5. Bone-specific skeletal tissue volumes for the 1-year-old skeleton calculated from the data shown in tables 1 and 2 and segmented in the 1-year-old skeleton.

1 year Skeletal region	Cortical bone (cm^3)	Spongiosa (cm^3)	RBM med (cm^3)	YBM med (cm^3)	Cart/misc (cm^3)	Total (cm^3)
Wrist and hand bones	5.74	5.84			6.30	17.88
Radii and Ulnae	10.33	3.45	2.40	0.30	12.61	29.08
Humeri, upper half	6.25	2.81	2.43	0.13	8.16	19.79
Humeri, lower half	6.25	3.26	2.07	0.26	8.16	20.00
Ribs	26.06	15.31			28.93	70.29
Sternum	2.01	1.35			2.23	5.58
Scapulae	6.68	4.57			7.42	18.67
Clavicles	2.34	1.38			2.60	6.31
Cervical vertebrae	1.87	9.89			7.79	19.54
Thoracic vertebrae	4.62	26.74			19.29	50.64
Lumbar vertebrae	5.32	16.91			16.32	38.55
Sacrum	7.39	5.54			9.64	22.57
Cranium	141.14	45.90			155.03	342.07
Mandible	14.18	4.43			15.58	34.18
Pelvis	11.52	18.29			13.35	43.16
Femora, upper half	9.05	6.54	4.20	0.22	14.09	34.11
Femora, lower half	9.05	7.27	3.57	0.44	14.09	34.42
Tibiae, fibulae, patellae	14.93	15.26	3.95	0.49	20.77	55.40
Ankle and foot bones	7.77	14.10			8.53	30.39
	292.48	208.84	18.61	1.83	370.88	892.64
ICRP89 (no teeth)						892.40

Tab 6. Organ and tissue masses for the newborn and 1-year-old ICRP89 reference children and for the voxelized paediatric phantoms P00 (M00, F00) and P01(M01, F01)

	Newborn male		Newborn female		1-year-old male		1-year-old female	
	ICRP89	M00	ICRP89	F00	ICRP89	M01	ICRP89	F01
ORGAN / TISSUE	(g)	(g)	(g)	(g)	(g)	(g)	(g)	(g)
Adipose	930.0	928.7	930.0	928.7	3800.0	3800.0	3800.0	3800.0
Adrenals	6.0	6.0	6.0	6.0	4.0	4.0	4.0	4.0
Tongue	3.5	3.5	3.5	3.5	10.0	10.0	10.0	10.0
Salivary Glands	6.0	6.0	6.0	6.0	24.0	24.0	24.0	24.0
Oesophagus wall	2.0	2.0	2.0	2.0	5.0	5.0	5.0	5.0
Stomach wall	7.0	7.0	7.0	7.0	20.0	20.0	20.0	20.0
Small Intestine wall	30.0	30.0	30.0	30.0	85.0	85.0	85.0	85.0
Colon wall	17.0	17.0	17.0	17.0	50.0	50.0	50.0	50.0
GI contents	144.0	144.0	144.0	144.0	240.0	244.0	240.0	244.0
Liver	130.0	130.0	130.0	130.0	330.0	330.0	330.0	330.0
Gallbladder wall	0.5	0.7	0.5	0.7	1.4	1.5	1.4	1.5
Gall bladder cont.	2.8	2.6	2.8	2.8	8.0	7.9	8.0	7.9
Pancreas	6.0	6.0	6.0	6.0	20.0	20.0	20.0	20.0
Brain	380.0	380.0	380.0	380.0	950.0	950.0	950.0	950.0
Breasts (glandular)	n.a.	0.09	n.a.	0.09	n.a.	0.26	n.a.	0.26
Heart wall	20.0	20.0	20.0	20.0	50.0	50.0	50.0	50.0
Blood [a]	290.0		290.0		530.0		530.0	
Eyes	6.0	6.0	6.0	6.0	7.0	7.0	7.0	7.0
Skin	175.0	175.3	175.0	175.2	350.0	350.4	350.0	350.0
Muscle	800.0	799.9	800.0	799.9	1900.0	1901.5	1900.0	1901.5
Larynx [b]	1.3	1.4	1.3	1.4	4.0	4.7	4.0	4.7
Trachea	0.5	0.5	0.5	0.5	1.5	1.5	1.5	1.5
Lungs	60.0	60.0	60.0	60.0	150.0	150.0	150.0	150.0
Skeleton	370.0	369.2	370.0	369.2	1170.0	1170.8	1170.0	1170.8
Spleen	9.5	9.5	9.5	9.5	29.0	29.0	29.0	29.0
Thymus	13.0	13.0	13.0	13.0	30.0	30.0	30.0	30.0
Thyroid	1.3	1.3	1.3	1.3	1.8	1.8	1.8	1.8
Kidneys	25.0	25.0	25.0	25.0	70.0	70.0	70.0	70.0
Bladder wall	4.0	4.0	4.0	4.0	9.0	9.0	9.0	9.0
Testes	0.85	0.8			1.5	1.5		
Prostate	0.8	0.8			1.0	1.0		
Ovaries			0.3	0.3			0.8	0.8
Uterus			4.0	4.0			1.5	1.5
Bronchi	n.a.	0.8	n.a.	0.8	n.a.	1.5	n.a.	1.5
Connective Tissue	120.0	70.5	120.0	70.5	350.0	240.4	350.0	240.4
Lymphatic Nodes	20.0	20.0	20.0	20.0	50.0	50.0	50.0	50.0
Other tissues [c]		263.0		263.0		367.5		367.5
Total body mass	3582.1	3504.6	3584.7	3507.4	10252.2	9989.3	10252.0	9988.7
Height (cm)	51.0	50.5[d]	51.0	50.5[d]	76.0	75.8	76.0	75.8

[a] without lungs

[b] Phantom: Larynx Pharynx

[c] includes soft tissue, blood, etc.

[d] Phantom legs not completely stretched

Segmented organ and tissue masses for male and female phantoms are shown in table 6 together with the ICRP89 reference masses. All important organ and tissue masses in the paediatric phantoms match the reference masses exactly, except for small differences for the skeletons, for example: 0.2% for the newborn and 0.1% for the 1-year-old phantoms. Only the main blood vessels have been segmented in the paediatric phantoms. Therefore, blood mass appears explicitly as well as implicitly (included in other tissues) in table 6. Finally, table 7 shows the skeletal tissue volumes of the P00 and the P01 phantoms together with the corresponding target volumes from table 1. Note that the skeletal tissue

volumes have not been adjusted to match the target volumes. Their values are the result of the calculation procedure described above, the segmentation of the μCT images into trabecular bone and marrow and of the marrow into RBM, YBM and bone endosteum (BE) in all spongiosa voxels of the skeletons at runtime of the MC code (Kramer et al 2010, 2012). As teeth begin to appear around 6-9 months (Gray 1977) they were segmented only in the 1-year-old P01 phantom. Although being hermaphrodite phantoms, organ masses for P00 and P01are shown in sex-specific columns.

Tab 7. Comparison between skeletal target volumes from table 1 and the calculated and segmented volumes in the P00 and the P01 skeletons.

	Newborn			One year		
Skeletal region	Target volume (cm^3)	P00 volume (cm^3)	Dif (%)	Target volume (cm^3)	P01 volume (cm^3)	Dif (%)
Bone, cortical	81.8	84.7	3.4	283.1	292.1	3.1
Bone, trabecular	21.2	23.6	10.2	72.3	73.9	2.2
Bone, total	103.0	108.3	4.9	355.4	366.0	2.9
Marrow, red (active)	48.5	43.6	-11.2	145.6	141.8	-2.7
Marrow, yellow (inactive)				20.4	17.3	-17.9
Cartilage	118.2	118.2	0.0	327.3	327.0	-0.1
Teeth	0.3			1.8	1.82	1.1
Miscellaneous	18.7	18.7	0.0	43.7	43.7	0.0
Total skeleton	288.7	288.8	0.0	894.2	897.6	0.4

3.2 Dosimetry

3.2.1 Dosimetric comparison with stylized phantoms

Seidenbusch et al (2008) published a comprehensive study on conversion coefficients (CCs) between organ and tissue absorbed dose and incident air kerma (INAK) for paediatric thorax examinations using PCXMC (http://www.stuk.fi/sateilyn_kaytto/ohjelmat/PCXMC/en_GB/pcxmc/). This commercial software performs MC calculations in the stylized MIRD5 phantoms (Cristy and Eckerman 1987) for newborns, 1, 5, 10, 15 years of age and for adults. Here, a comparison will be made between radiographs of the thorax with posterior-anterior (PA) projection, 60 kV and 80 kV X-ray spectra with 13^0 anode angle, 3.5 mm Al + 0.1 mm Cu filtration and focus-detector-distance (FDD) of 150 cm for newborns and 1-year-old infants. Figures 11 and 12 show the exposure geometries for the P00 (newborn) and the P01 (1-year-old) phantoms, respectively, while size and position of the radiation fields used for the MIRD5 phantoms are presented in figure 13. Statistical errors (= one standard deviation) were less than 1% for organs located in the X-ray beam volume in both studies.

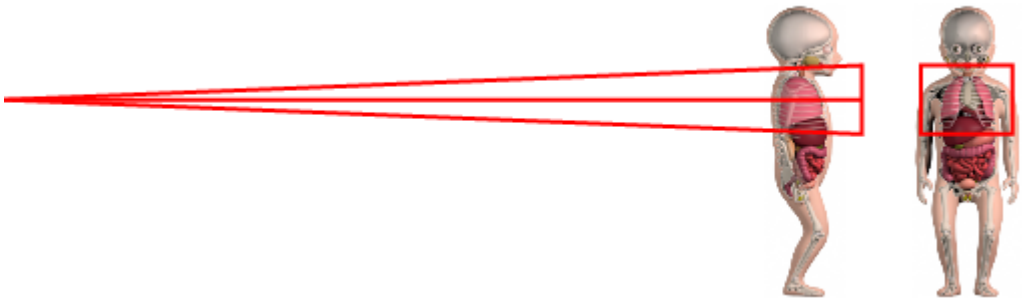

Fig 11. P00 phantom: Exposure geometry for thorax examination. Filed size in receptor plane = 16 cm x 12 cm

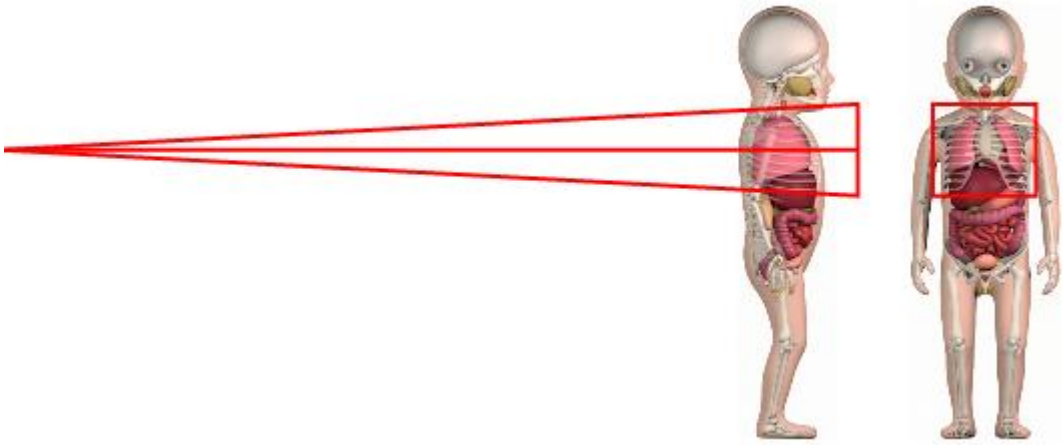

Fig 12. P01 phantom: Exposure geometry for thorax examination. Filed size in receptor plane = 18 cm x 16 cm

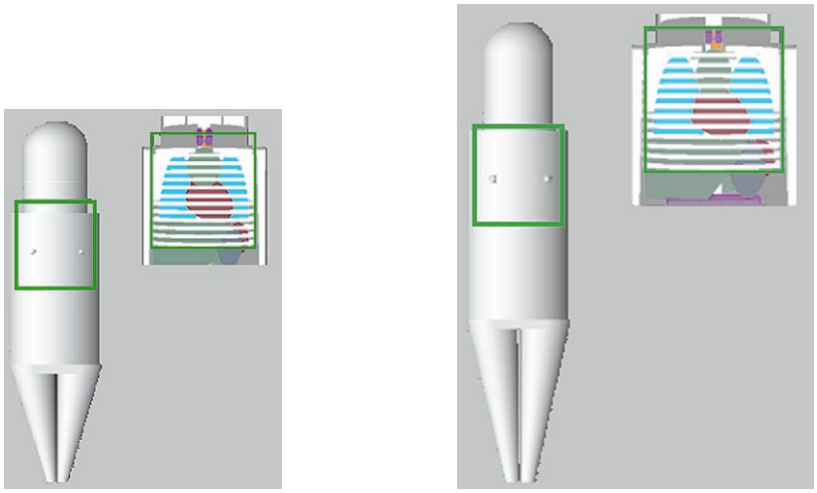

Fig 13. Newborn (left) and 1-year-old (right) MIRD5 phantoms: Frontal view with radiation field position for thorax examination PA as used by Seidenbusch et al (2008).

The results presented in table 8 show good agreements between the CCs for the different phantoms for the liver, the lungs, the stomach and the effective dose (ICRP 2007). Reasonable agreement can still be observed for oesophagus and spleen. For other organs the differences between CCs are larger because of the anatomical differences between the phantoms which become evident when comparing figures 11 and 12 with figure 13 or because of the position of organs relative to the X-ray beam. For example, in the P00 and P01 phantoms, the kidneys are located outside the X-ray beam while in the MIRD5 phantoms they are located partly inside the beam. The contrary holds for the thyroid. The unrealistic geometrical structure of the MIRD5 ribcage which provides more shielding is the cause of the breast, thymus and heart wall absorbed doses being smaller than the corresponding P00/P01 data. The lung densities are 0.29 g cm^{-3} and 0.25 g cm^{-3} for the MIRD5 and the P00/P01 phantoms, respectively. This compensates the "ribcage effect" for the MIRD5 lungs and therefore its absorbed doses agree well with the P00/P01 values. Effective doses for the P00/P01 and the MIRD5 phantoms agree well.

Tab 8. Organ and tissue absorbed doses D_T normalized to incident air kerma K_a for thorax PA radiographs for newborn and 1-year-old infants, calculated with the P00, P01 and MIRD5 phantoms. The MIRD5 data were taken for the small field from table 8 of the work of Seidenbusch et al (2008).

Thorax PA 3.5 mm Al + 0.1 mm Cu	NEWBORN				ONE YEAR			
	60 kV		80 kV		60 kV		80 kV	
	P00	MIRD5	P00	MIRD5	P01	MIRD5	P01	MIRD5
	D_T/K_a Gy/Gy	D_T/K_a Gy/Gy	D_T/K_a Gy/Gy	D_T/K_a Gy/Gy	D_T/K_a Gy/Gy	D_T/K_a Gy/Gy	D_T/K_a Gy/Gy	D_T/K_a Gy/Gy
ADRENALS	0.42	0.79	0.49	0.90	0.32	0.72	0.39	0.85
BREAST, Glandular	0.41	0.28	0.51	0.36	0.19	0.20	0.25	0.28
KIDNEYS	0.08	0.31	0.10	0.36	0.07	0.15	0.10	0.18
LIVER	**0.34**	**0.32**	**0.42**	**0.40**	**0.22**	**0.23**	**0.28**	**0.30**
LUNGS	**0.84**	**0.80**	**0.94**	**0.91**	**0.71**	**0.70**	**0.83**	**0.83**
OESOPHAGUS	0.61	0.43	0.73	0.57	0.48	0.37	0.60	0.52
SPLEEN	0.50	0.64	0.56	0.73	0.34	0.45	0.41	0.54
STOMACH WALL	**0.24**	**0.23**	**0.30**	**0.30**	**0.18**	**0.14**	**0.23**	**0.20**
THYMUS	0.42	0.20	0.52	0.28	0.23	0.15	0.31	0.22
THYROID	0.46	0.17	0.58	0.24	0.16	0.13	0.22	0.20
HEART WALL	0.54	0.37	0.64	0.47	0.37	0.27	0.48	0.37
EFFECTIVE DOSE	**0.27**	**0.28**	**0.32**	**0.34**	**0.20**	**0.22**	**0.24**	**0.28**

3.2.2 Dosimetric comparison with the newborn voxel phantom BABY

The phantoms BABY and CHILD, developed by Williams et al (1986), are the first whole-body voxel phantoms based on tomographic images of human bodies. In that project, whole body CT scans were made from an 8-week-old cadaver and from a 7-year-old leukaemia patient who was scheduled for whole body gamma irradiation prior to a bone marrow transplant. Specific information on the construction of the phantoms is given in Veit et al (1989). For the comparison with the paediatric phantoms P00, data from the report by Zankl et al (1993) on paediatric CCs for BABY for computed tomography (CT) were used. The report contains average organ and tissue absorbed doses normalized to air kerma free in air at the centre of rotation. The phantom was scanned from top to toe with consecutive X-ray beams of 1 cm width. Beam shaping devices, such as bow-tie filters, and tube-current modulation were not taken into account. The BABY phantom has original organ and tissue masses according to the tomographic images, i.e. they have not been adjusted to the organ and tissue masses given by ICRP89 (ICRP2002). Body mass and height are 3.5 kg/50.5 cm and 4.2 kg/57 cm for P00 and BABY, respectively. Both phantoms, P00 and BABY, are shown in figure 14. The arms have not been removed during simulation.

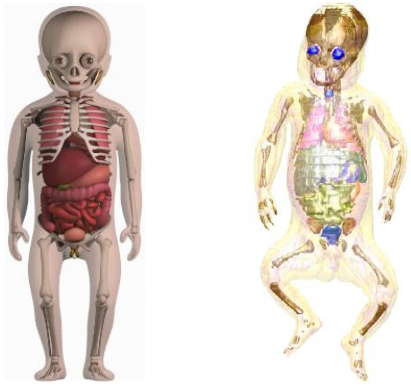

Fig 14. Newborn phantoms P00 (left) and BABY (right).The image of the BABY phantom was taken from the work of Schlattl et al (2012)

Tab 9. Organ and tissue absorbed doses D_T normalized to air kerma K_a at the centre of rotation for the phantoms P00 and BABY for one rotation at the liver centre of mass. The BABY CCs were taken from Zankl et al (1993), appendix B, slice 23 to 24 for 360^0 rotation. The statistical errors given by the MC codes are also shown together with the percentage differences between P00 and BABY data.

	80 kV					125 kV				
Liver CT	P00		BABY			P00		BABY		
2.2mm Al + 0.2mm Cu	D_T/K_a	Error	D_T/K_a	Error	Dif	D_T/K_a	Error	D_T/K_a	Error	Dif
1 rotation at CoM	Gy/Gy	%	Gy/Gy	%	%	Gy/Gy	%	Gy/Gy	%	%
KIDNEYS	0.028	0.92	0.017	1.17	39.3	0.032	0.89	0.021	1.17	34.4
LIVER	**0.159**	**0.17**	**0.149**	**0.20**	**6.3**	**0.181**	**0.17**	**0.168**	**0.20**	**7.2**
LUNGS	**0.025**	**0.63**	**0.024**	**0.85**	**4.0**	**0.028**	**0.62**	**0.029**	**0.85**	**-3.6**
SI WALL	**0.010**	**1.43**	**0.010**	**1.34**	**0.0**	**0.011**	**1.35**	**0.012**	**1.34**	**-9.1**
SPLEEN	**0.197**	**0.57**	**0.189**	**0.61**	**4.1**	**0.223**	**0.56**	**0.212**	**0.61**	**4.9**
STOMACH WALL	0.122	0.75	0.098	1.40	19.7	0.135	0.72	0.109	1.40	19.3
THYMUS	**0.010**	**2.16**	**0.009**	**2.23**	**10.0**	**0.012**	**2.05**	**0.011**	**2.23**	**8.3**
THYROID	**0.004**	**9.44**	**0.004**	**10.23**	**0.0**	**0.005**	**9.54**	**0.005**	**10.23**	**0.0**
CoM: Centre of mass				average:	10.4				average:	10.8
SI: Small intestine										

Table 9 presents organ and tissue absorbed doses D_T normalized to air kerma K_a at the centre of rotation for the phantoms P00 and BABY for one rotation at the liver centre of mass with 1 cm slice thickness for two different X-ray spectra. Most differences are smaller than 10%, except for kidneys and stomach, two organs which are known for having sometimes quite different positions in the abdominal region of different individuals (Cassola et al 2010b). Average differences are 10.4% and 10.8% for 80 kV and 125 kV, respectively, which can be considered as good agreement.

3.2.3 Dosimetric comparison with the newborn NURBS-based phantom of the University of Florida

Developed by Lee et al (2007) as the first NURBS-based, hybrid computational phantoms, the newborn male and female models of the University of Florida (UFNHP) were used by Pafundi et al (2009, 2010) to calculate specific absorbed fractions (SAFs) in the target tissues red bone marrow (RBM) and bone endosteum (BE) from electrons isotropically emitted in various skeletal source tissues. Both phantoms, P00 and UFNHP, are shown in figure 15.

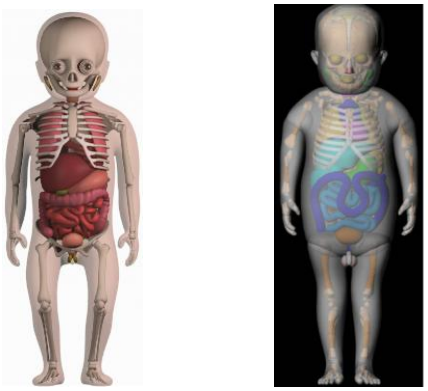

Fig 15. Newborn phantoms P00 (left) and UFNHP (right). The image of the male UFNHP phantom was taken from the work of Lee et al (2007b)

The comparison between P00 and UFNHP SAFs will be presented for the pelvis with the RBM as the source tissue, which is equivalent to BM being the source tissue because cellularity is 100% in newborns (ICRP 1995). Statistical errors (= one standard deviation) were below 1% for both, the DEN and the UF calculations. The UFNHP data have been taken from tables A31 and A32 of the Annex A of the paper of Pafundi et al (2010). Figure 16 presents SAFs in the red bone marrow (RBM) and the bone endosteum (BE) of the pelvis from electrons emitted in the RM volume as a function of the particle energy from 10 keV to 4 MeV for the P00 and the University of Florida newborn (UFNHP) phantoms. Reasonable agreement between P00 and UFNHP SAFs can be observed, but to better compare the results for the two phantoms the data are additionally presented in table 10 together with the percentage differences between them. Most differences are around 10% or smaller, except for energies between 200 and 500 keV. In this energy region, electrons emitted in the marrow cavities start penetrating the adjacent bone trabeculae to deposit a part of their kinetic energy in neighbouring marrow cavities (Kramer et al 2010). The trabecular bone volume fraction (TBVF) in the pelvis of the UFNHP phantom is 0.4112 (Pafundi et al 2009), while the pelvis TBVF of the P00 phantom is 0.207, which is the TBVF for the 5-year-old F05/M05 phantoms (de Melo Lima et al 2010). From the TBVF difference one can conclude that the UFNHP pelvis has thicker trabeculae and smaller marrow cavities than the P00 pelvis which explains the difference of the SAFs between 200 and 500 keV. For higher energies, especially above 1 MeV, the flux of electrons through trabeculae and cavities becomes independent of the TBVF and consequently all SAFs agree well. Over the whole energy range, the absolute average differences are 8.50% and 6.05% for the RBM and BE SAFs, respectively.

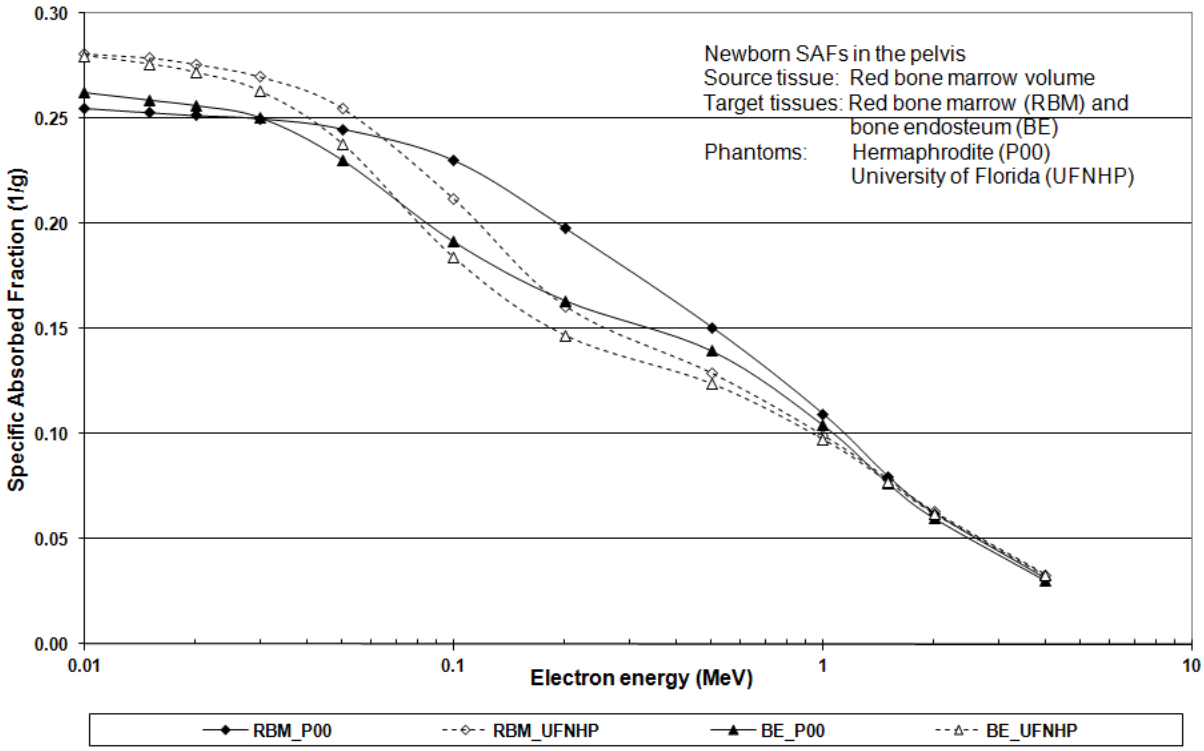

Fig 16. Specific absorbed fractions in the red bone marrow (RBM) and the bone endosteum (BE) of the pelvis from electrons emitted in the RM volume as a function of the particle energy from 10 keV to 4 MeV for the P00 and the University of Florida newborn (UFNHP) phantoms.

Tab 10. Specific absorbed fractions in the red bone marrow (RBM) and the bone endosteum (BE) of the pelvis from electrons emitted in the RBM volume as a function of the particle energy from 10 keV to 4 MeV for the P00 and the University of Florida newborn (UFNHP) phantoms. The table shows the graphs from figure 12 together with percentage differences.

Pelvis Source Target E (MeV)	P00 RMVOL RBM SAF (g^{-1})	UFNHP RMVOL RBM SAF (g^{-1})	RBM Dif (%)	P00 RMVOL BE SAF (g^{-1})	UFNHP RMVOL BE SAF (g^{-1})	BE Dif (%)
0.01	**2.55E-01**	**2.81E-01**	**-10.20**	**2.63E-01**	**2.80E-01**	**-6.63**
0.015	**2.53E-01**	**2.79E-01**	**-10.28**	**2.59E-01**	**2.76E-01**	**-6.56**
0.02	**2.52E-01**	**2.76E-01**	**-9.70**	**2.56E-01**	**2.72E-01**	**-6.08**
0.03	**2.50E-01**	**2.70E-01**	**-7.96**	**2.51E-01**	**2.63E-01**	**-4.95**
0.05	**2.45E-01**	**2.55E-01**	**-4.00**	**2.30E-01**	**2.38E-01**	**-3.30**
0.1	**2.30E-01**	**2.12E-01**	**7.95**	**1.92E-01**	**1.84E-01**	**3.97**
0.2	1.98E-01	1.61E-01	18.69	1.65E-01	1.47E-01	10.91
0.5	1.51E-01	1.29E-01	14.46	1.40E-01	1.24E-01	11.17
1.0	**1.10E-01**	**9.94E-02**	**9.22**	**1.04E-01**	**9.76E-02**	**6.42**
1.5	**7.97E-02**	**7.85E-02**	**1.48**	**7.66E-02**	**7.74E-02**	**-1.11**
2.0	**6.22E-02**	**6.30E-02**	**-1.27**	**6.00E-02**	**6.22E-02**	**-3.70**
4.0	**3.11E-02**	**3.32E-02**	**-6.79**	**3.02E-02**	**3.28E-02**	**-8.50**
		average:	8.50		average:	6.05

4. Conclusion

Using the methods developed by Cassola et al (2010) and by de Melo Lima et al (2011), this study has presented hermaphrodite paediatric phantoms for newborn and 1-year-old infants in mesh and voxel format based on anatomical information from atlases, textbooks, cadaver images from the Department of Anatomy of the UFPE and documents of the ICRP and the ICRU. The anatomical models are called "reference phantoms" because their organ and tissue masses have been adjusted to the corresponding reference masses given by ICRP89 (ICRP 2002). Most of the organ and tissues masses of the P00 and the P01 phantoms match the target masses exactly. Although not mentioned by ICRP89 in table 2.8, breast tissue was segmented in all paediatric DEN phantoms. Whole body skeletal tissue masses given by ICRP89 were distributed among bones using data from ICRP89 and ICRP70 (ICRP 1995) to derive bone-specific target volumes. Segmentation of the skeleton into cortical bone, spongiosa, cartilage and medullary marrow and application of μCT images of trabecular bone made it possible to match most skeletal tissue target masses within a margin of less than 10%. Using sophisticated 3D modelling methods it was possible to create anatomically realistic mesh bodies, organs and skeletons and to maintain this feature for the voxel format by using a small voxel size of 0.07cm x 0.07cm x 0.07cm. The phantoms P00 and P01 are comprehensively presented in images and data tables.

Three comparative calculations have shown that the newborn (P00) and the 1-year-old (P01) phantoms provide reasonable dosimetric results. The comparison with the MIRD5 CCs for thorax examinations (Seidenbusch et al 2008) showed excellent agreement for the lungs, the liver, the stomach and effective dose, and reasonable agreement for the oesophagus and the spleen. Significant differences between MIRD5 and P00/P01 CCs could be explained with reference to anatomical differences and/or different organ positions relative to the edge of the radiation field. The dosimetric comparison between the P00 and the BABY voxel phantoms for a single liver CT scan showed generally good agreement with an average percentage difference of 10.6%. Even smaller differences were found for the comparison between the P00 and UFNHP, both newborn reference voxel phantoms and both using μCT images of trabecular bone for skeletal dosimetry. Average percentage differences were 8.5% and 6.05% for RBM and BE electron SAFs, respectively, when the (red) marrow volume is the source tissue.

This study has a limitation with respect to the skeletal dosimetry method. As μCT images of trabecular bone for newborn and 1-year-old infants are currently not available, anatomical and dosimetric results for skeletal tissues are partly based on adult data. In view of this limitation, the comparisons of the skeletal tissue volumes in table 7 and of the SAFs in table 10 can be considered as reasonable, also because no attempt was made to adjust the skeletal tissue volumes to match the reference volumes exactly. The aim of the DEN research program on skeletal dosimetry is to eventually use age-specific paediatric μCT images of trabecular bone and cortical-to-trabecular bone ratios in the future and to update the corresponding phantoms and MC codes as soon as this data becomes available.

Bold numbers in tables 8, 9 and 10 indicate good agreement with the data from others.

5. Acknowledgement

The authors would like to thank the Conselho Nacional de Desenvolvimento Científico e Tecnológico - CNPq and the Fundação de Amparo à Ciência do Estado de Pernambuco - FACEPE for financial support. Special thanks go to Dr. Seidenbusch, University of Munich, Germany,for providing the images for figure 13 and to Dr. Carlos Vieira from the Porto Seguro Diagnostic Medical Centre in Porto Seguro, Bahia, Brazil for providing the CT images shown in figures 9 and 10.

6. References

Brenner D J, Elliston C D, Hall E J and Berdon W E 2001 Estimated Risks of Radiation-Induced Fatal Cancer from Pediatric CT, *Am J Roent* **176** 289-296

Cassola V F, de Melo Lima V J, Kramer R and Khoury H J 2010a FASH and MASH: Female and Male Adult human phantoms based on polygon meSH surfaces. Part I: Development of the anatomy *Phys Med Biol* **55** 133-162

Cassola V F, Kramer R, Brayner C and Khoury H J 2010b Posture-specific phantoms representing female and male adults in Monte Carlo-based simulations for radiological protection, *Phys Med Biol* **55** 4399-4430

Cassola V F, Milian F M, Kramer R, de Oliveira Lira C A B and Khoury H J 2011 Standing adult human phantoms based on 10^{th}, 50^{th} and 90^{th} mass and height percentiles of male and female Caucasian populations, *Phys Med Biol* **56** 3749-3772

Cranley K Gilmore B J Fogarty G W A and Desponds L 1997 Catalogue of Diagnostic X-ray Spectra and Other Data the Institute of Physics and Engineering in Medicine (IPEM) Report No. 78 Electronic version prepared by D.Sutton September 1997

Christ A, Kainz W, Hahn E G, Honegger K, Zefferer M, Neufeld E, Rascher W, Janka R, Bautz W, Chen J, Kiefer B, Schmitt P, Hollenbach H-P, Shen J, Oberle M, Szczerba D, Kam A, Guag J W and Kuster N 2010 The virtual family – development of surface-based models of two adults and two children for dosimetric simulations *Phys Med Biol* **55** N23-N38

Cristy M 1980 Mathematical phantoms representing children of various ages for use in estimates of internal dose, *Oak Ridge National Laboratory Report* ORNL/NUREG/TM-367

Cristy M and Eckerman K F 1987 Specific absorbed fractions of energy at various ages from internal photon sources, *Oak Ridge National Laboratory Report* ORNL/TM-8381/V1

de Melo Lima V J, Cassola V F, Kramer R, de Oliveira Lira C A B, Khoury H J and Vieira J W 2011 Development of 5- and 10-year-old pediatric phantoms based on polygon mesh surfaces, *Med Phys* **38** (8) 4723-4736

Gray H 1977Anatomia, 29. Edition Guanabara Koogan, Rio de Janeiro

Han E Y, Bolch W E and Eckerman K F 2006 Revisions to the ORNL series of adult and pediatric computational phantoms for use with the MIRD schema, *Health Physics*, **90**(4) 337-356

ICRP 1995 Basic Anatomical and Physiological Data for use in Radiological Protection: The Skeleton. *ICRP Publication* **70** Ann. ICRP 25 (2) Oxford: Pergamon

ICRP 2002 Basic Anatomical and Physiological Data for Use in Radiological Protection: Reference Values", *ICRP Publication* **89**, Ann. ICRP 32(3-4) Pergamon, Oxford

ICRP 2007 Recommendations of the International Commission on Radiological Protection, *ICRP Publication* **103** Ann. ICRP 37 (2-4) Pergamon, Oxford

ICRU 1992 International Commission on Radiation Units and Measurements, Photon, Electron, Proton and Neutron Interaction Data for Body Tissues, ICRU Report 46, Bethesda, Maryland, USA

Kawrakow I and Rogers D W O 2003 The EGSnrc code system: Monte Carlo simulation of electron and photon transport, *NRC Report PIRS-701*, version V4-2.3.1, available at http://irs.inms.nrc.ca/software/egsnrc/

Kramer R, Vieira J W, Khoury H J, Lima F R A and Fuelle D 2003 All About MAX: a Male Adult voXel Phantom for Monte Carlo Calculations in Radiation Protection Dosimetry", *Phys Med Biol* **48** 1239-1262

Kramer R, Vieira J W, Khoury H J, Lima F R A, Loureiro E C M, Lima V J M and Hoff G 2004 All about FAX: a Female Adult voXel Phantom for Monte Carlo Calculation in Radiation Protection Dosimetry, *Phys Med Biol* **49** 5203-5216

Kramer R, Khoury H J, Vieira J W and Lima V J M 2006a MAX06 and FAX06: Update of two adult human phantoms for radiation protection dosimetry, *Phys Med Biol* **51** 3331-3346

Kramer R, Khoury H J, Vieira J W and Kawrakow I 2006b Skeletal dosimetry in the MAX06 and the FAX06 phantoms for external exposure to photons based on vertebral 3D-microCT images, *Phys Med Biol.* **51** 6265-6289

Kramer R, Khoury H J, Vieira J W and Kawrakow I 2007 Skeletal dosimetry for external exposure to photons based on μCT images of spongiosa from different bone sites, *Phys Med Biol*. ***52*** 6697-6716
Kramer R, Khoury H J, Vieira J W and Robson Brown K A 2009 Skeletal dosimetry for external exposures to photons based on μCT images of spongiosa: Consideration of voxel resolution, cluster size and medullary bone surfaces *Med Phys* **36** 11 5007-5016
Kramer R, Cassola V F, Khoury H J, Vieira J W, de Melo Lima V J and Robson Brown K 2010 FASH and MASH: female and male adult human phantoms based on polygon mesh surfaces: II. Dosimetric calculations, *Phys Med Biol* **55** 163-189
Kramer R, Richardson R B, Cassola V F, Vieira J W, Khoury H J, de Oliveira Lira C A B and Robson Brown K 2011 Electron absorbed fractions of energy and S-values in an adult skeleton based on μCT images of trabecular bone, *Phys Med Biol* **56** 1803-1836
Kramer R, Cassola V F, Vieira J W, Khoury H J, de Oliveira Lira C A B and Robson Brown K 2012 Skeletal dosimetry based on μCT images of trabecular bone: update and comparisons, *Phys Med Biol* **57** 3995-4021
Lee C, Williams J L, Lee C and Bolch W E 2005 The UF series of tomographic computational phantoms of pediatric patients, *Med Phys* **32**(12) 3537-3548
Lee C, Lee C, Williams J L and Bolch W E 2006 Whole-body voxel phantoms of pediatric patients – UF series B, *Phys Med Biol* **51** 4649-4661
Lee C, Lee C, Han E Y and Bolch W E 2007a Considerations of the ICRP 2006 revised tissue weighting factors on age-dependent values of the effective dose for external photons, *Phys Med Biol* **52** 41-58
Lee C, Lodwick D, Hasenauer D, Williams J L, Lee C and Bolch W E 2007b Hybrid computational phantoms of the male and female newborn patient: NURBS-based whole-body models, *Phys Med Biol* **52** 3309-3333
Lee C, Lodwick D, Williams J L and Bolch W E 2008 Hybrid computational phantoms of the 15-year male and female adolescent: Application to CT organ dosimetry for patients of variable morphometry, *Med Phys* **35**(6) 2366-2382
Lee C, Lodwick D, Hurtado J, Pafundi D, Williams J L and Bolch W E 2010 The UF family of reference hybrid phantoms for computational radiation dosimetry, *Phys Med Biol* **55** 339-363
MacGregor J 2000 Introduction to the anatomy and physiology of children, Rouledge, London
Moore K L and Dalley A F 2007 Anatomia orientada para a clínica, 5. Edition, Guanabara Koogan, Rio de Janeiro
Nagaoka T, Kunieda E and Watanabe S 2008 Proportion-corrected scaled voxel models for Japanese children and their application to the numerical dosimetry of specific absorption rate for frequencies from 30 MHz to 3 GHz, *Phys Med Biol* **53** 6695-6712
Netter F H 1999 Atlas Interativo de Anatomia Humana, Novartis Medical Education, Editor Artmed, Porto Alegre, Brazil
Pafundi D, Lee C,Watchman C, Bourke V, Aris J, Shagina M, Harrison J, Fell T and Bolch W 2009 An image-based skeletal tissue model for the ICRP reference newborn, *Phys Med Biol* **54** 4497-4531
Pafundi D, Rajon D, Jokisch D, Lee C and Bolch W 2010 An image-based skeletal tissue model for the ICRP reference newborn – internal electron sources, *Phys Med Biol* **55** 1785-1814
Rosendaal T 2009 Blender 2.49b, http://www.blender.org/
Schlattl H, Zankl M, Becker J and Hoeschen C 2012 Dose conversion coefficients for paediatric CT examinations with automatic tube current modulation, *Phys Med Biol* **57** 6309-6326
Seidenbusch M C, Regulla D and Schneider K 2008 Zur Strahlenexposition von Kindern in der pädiatrischen Radiologie, Teil 3: Konversionsfaktoren zur Rekonstruktion von Organdosen bei Thoraxaufnahmen, *Fortschr Röntgenstr* **180** 1061-1081
Snyder G, Schneider L W, Owings C L, Reynolds H M, Golomb D H and Schork M A 1977 Antropometry of infants, children and youths to age 18 for product safety design, Report UM-HSRI-77-17, U. S. Consumer Product Safety Commission: Bethesda, available at http://ovrt.nist.gov/projects/anthrokids/

Veit R, Zankl M, Petoussi N, Mannweiler E, Williams G and Drexler G 1989 Tomographic anthropomorphic models, Part I: Construction technique and description of models of an 8 week old baby and a 7 year old child. GSF-Report 3/89, Gesellschaft für Strahlen- und Umweltforschung mbH, München, Germany

Williams G, Zankl M, Abmayr W, Veit R and Drexler G 1986 The calculation of dose from external exposures using reference and realistic human phantoms and Monte Carlo methods, *Phys Med Biol* **31** 449-452

Xu X G and Eckerman K F 2010 Handbook of Anatomical Models for Radiation Dosimetry, CRC Press, Taylor and Francis, Boca Raton, FL, USA

Zankl M, Veit R, Williams G, Schneider K, Fendel H, Petoussi N and Drexler G 1988 The construction of computer tomographic phantoms and their application in radiology and radiation protection, *Radiat Environ Biophys* **27** 153-164

Zankl M, Panzer W and Drexler G 1993 Tomographic Anthropomorphic Models, Part II: Organ Doses from Computed Tomographic Examinations in Peadiatric Radiology, Institut für Strahlenschutz, GSF-Report 30/93, GSF – Forschungszentrum für Umwelt und Gesundheit